RSC Advances

PAPER

View Article Online
View Journal | View Issue

Cite this: *RSC Adv.*, 2014, **4**, 30180

Geometric effect of Ru/HSAG@mSiO$_2$: a catalyst for selective hydrogenation of cinnamaldehyde

Hangjia Shen, Haodong Tang,* Haiyu Yan, Wenfeng Han, Ying Li and Jun Ni*

Received 21st May 2014
Accepted 27th June 2014

DOI: 10.1039/c4ra04811c

www.rsc.org/advances

A new strategy to synthesize a catalyst consisting of graphite-supported Ru nanoparticles encapsulated by mesoporous silica layers was developed *via* a facile and scalable wet-chemical process. The intended structures were confirmed with N_2 sorption, CO chemisorption, TEM and SEM. The geometric effect of the pores in the silica layer of Ru/HSAG@mSiO$_2$ was evaluated in the hydrogenation of cinnamaldehyde and showed 15% higher selectivity to unsaturated alcohol and three times higher turnover frequency (TOF) relative to unconfined Ru/HSAG catalyst with the equivalent size of Ru particles.

Introduction

With the development of mesoporous materials, they have found their increasing applications in protein separation, catalysis, environment protection, and photonic crystals, due to their extremely high surface areas combined with large and uniform pore sizes.[1] In catalysis, mesoporous materials have been used as novel functional materials for selective adsorption and to confine guest molecules in reactions where selectivity is highly required. When mesoporous materials are used as a coating of nanoparticles, they are able to not only prevent these nanoparticles from aggregating in reactions, but also improve catalytic selectivity due to the geometric and electronic effects of pores in mesoporous materials.[2–5]

It is known that the hydrogenation of cinnamaldehyde is a typical model reaction to investigate the effect of geometric structure of catalysts on selectivity.[6] Richard reported that the chemioselectivity in cinnamaldehyde hydrogenation could be greatly improved by using Pt and Rh metal clusters encapsulated in Y-type zeolites, because shape-selectivity effects in the zeolite micropores impose an end-on adsorption of the molecule *via* the C=O group on the encapsulated metal.[7] However, this conclusion was drawn without taking the effect of particle morphology into account, as the same author demonstrated in his later paper that high selectivity of unsaturated alcohol could be achieved with increasing the particle size of Pt and Rh metals. The effect of metal particle size is because a steric effect of the phenyl group hampers the molecule to adsorb parallel to the flat metal surface thus favouring the adsorption and hydrogenation of the C=O group with respect to the C=C group on large facetted metal particles.[8] Analogous effect of metal particle size was also reported in several literature using various metals, such as Pt,[9] Cu,[10] Ru.[11–13] In comparison with Pt catalysts which has high affinity towards C=C bond hydrogenation,[14] Ru catalysts have showed good selectivity in cinnamaldehyde hydrogenation as well as high activity.[15,16] A very high selectivity to cinnamyl alcohol (92% selectivity up to 80% conversion) was obtained on multilayer graphitic nanotube supported Ru catalysts, whereas a 20–30% selectivity on Ru/$A1_2O_3$ catalyst with similar-sized Ru particles was observed under the same conditions.[17]The enhancement of selectivity are likely attributed to the geometric effect of the graphitic nanotube, while the improvement of activity can be ascribed to the electronic effect of the graphite support that graphite can serve as the electron donor to enrich the electron densities of metals as a result leading to the high hydrogenation rates.[6]

Although the high surface area graphite appears to be a desired support of metal-supported catalysts for cinnamaldehyde hydrogenation to unsaturated alcohol,[8,18] there is still a challenge to synthesize a catalyst combining the merits of both geometric and electronic effects together. Herein, we report a facile and scalable wet-chemical process to prepare graphite-supported metal nanoparticles covered with a mesoporous silica layer (Ru/HSAG@mSiO$_2$). The Ru nanoparticles, supported on the graphite, are confined at the bottom of the pores in mSiO$_2$ layers. Due to the geometric effect that mSiO$_2$ imposed on the catalyst, with the equivalent size of Ru particles, Ru/HSAG@mSiO$_2$ with respect to Ru/HSAG afforded a 15% increase in unsaturated alcohol selectivity in cinnamaldehyde hydrogenation.

Experimental section

Catalyst preparation

Chemicals. All chemicals were analytical grade and used as received without further purification. High surface area graphite (HSAG 300 with D_{90} = 32.1 μm) was obtained from Timcal Ltd. (Switzerland). Tetraethyl orthosilicate (TEOS) and

Institute of Industrial Catalysis, Zhejiang University of Technology, Hangzhou 310014, Zhejiang, P. R. China. E-mail: tanghd@zjut.edu.cn; Junni@zjut.edu.cn; Fax: +86-571-88320930; Tel: +86-571-88320092

hexadecyltrimethylammonium bromide (C_{16}TAB) was purchased from GuibaoC.Ltd. (Hangzhou, China) and Shanghai Bioscience & Technology Co. Ltd. (Shanghai, China), respectively.

Synthesis of Ru/HSAG. High surface area graphite was used as the support to prepare catalyst by mechanical ball milling method. Briefly, mix the graphite with Ru_3CO_{12} in a casting can with 2 big iron balls (diameter 20 mm), 14 middle ones (diameter 10 mm) and 24 small ones (diameter 6 mm) at 200 rounds per minute for 1 hour. The obtained product was then reduced in H_2 at 300 °C for 60 min, denoted as Ru/HSAG.

Synthesis of Ru/HSAG@mSiO$_2$. The composite was prepared through a surfactant-directed sol–gel coating process by using CTAB as a template. Typically, a suspension in water containing Ru/HSAG particles (0.2 g) was dispersed in a mixture solution composed of CTAB (0.14 g), water (40 g), ethanol (24 g), and ammonia (2.5 mL) under ultrasonic treatment for 30 min. Then, TEOS (1.00 mL) was added drop wisely and stirred for 4 h at 25 °C. The as-made composite was collected by filtration and washed with water and ethanol, respectively, and then extracted by HCl–ethanol (2 mL/50 mL) solution to remove the surfactant CTAB, washed with water and ethanol again. Finally, the composite was dried at room temperature under vacuum for 12 h, denoted as Ru/HSAG@mSiO$_2$. The sample of directly dried of as-made composites at room temperature under vacuum for 12 h without any wash was denoted as Ru/HSAG@mSiO$_2$-w.

Catalyst characterization

Nitrogen adsorption–desorption measurement was performed at −196 °C using an NOVA 1000e (Quantachrome Instruments) micromeritics system. Before the measurement, the catalysts were outgassed in vacuum at 200 °C for 12 h. The Brumauer–Emmett–Teller (BET) method was utilized to calculate the specific surface areas. The pore size distribution derived from the adsorption branches of the isotherms was calculated by the DFT (Density Functional Theory) method, and the total pore volumes (V_t) were estimated from the adsorbed amount at a relative pressure P/P_0 of 0.995. The micro-mesopore volume and surface area were calculated by the *t*-plot method at relative pressure P/P_0 between 0.3 and 0.5.

The dispersion of Ru was obtained by CO chemisorption method, which was carried out at 40 °C on a Quantachrome Autosorb-1/C chemisorb apparatus. Prior to measurements, the catalysts were reduced *in situ* for 10 min at 200 °C in H_2. The metal dispersion was estimated based on the assumptions of a spherical geometry of the particles and a stoichiometric adsorption of one CO molecule on one Ru surface atom.

Thermogravimetric (TG) analyses were conducted on a NETZSCH STA449C from 40 °C to 500 °C (10 °C min^{-1}) under flowing argon (99.99%, 20 mL min^{-1}).

Transmission electron microscopy (TEM) experiments were carried out on a Tecnai G2 F30 S-Twin (Netherlands) operated at 200 kV. The samples for TEM measurements were dispersed in ethanol and then supported onto a lacey carbon film on a copper grid.

SEM studies were carried out by using a Hitachi S-4700 at 300 kV, the samples were pretreated by metal spraying.

Hydrogenation of cinnamaldehyde

The reaction mixture composed of 0.05 g Ru/HSAG (0.12 g Ru/HSAG@mSiO$_2$), 1.0 mL cinnamaldehyde, and 50 mL isopropanol, was introduced into a 250 mL autoclave. Prior the reaction, the autoclave was purged with hydrogen, and then the reaction was performed at 100 °C and 4.0 MPa hydrogen pressure with vigorous stirring at 1000 rpm. The reaction progress was monitored by taking approximate 0.50 mL samples at different time intervals for quantitative analysis on an SHIMADZU 2014 GC equipped with a FID detector and a HP-5 capillary column. Only CALD, HCAL, HCOL and COL are detected in the reaction products. The conversion and selectivity were determined by area normalization method and calculated with the formulas as below, where *A* is the peak area:

$$\text{Conversion}_{\text{CALD}} = \left(1 - \frac{A_{\text{CALD}}}{A_{\text{CALD}} + A_{\text{CALC}} + A_{\text{HCAD}} + A_{\text{HALC}}}\right) \times 100\%$$

$$\text{Selectivity}_{\text{CALC}} = \left(\frac{A_{\text{CALC}}}{A_{\text{CALC}} + A_{\text{HCAD}} + A_{\text{HALC}}}\right) \times 100\%$$

Results

Structure of catalysts

Nitrogen sorption isotherms and pore size distribution of catalysts are presented in Fig. 1. In addition to the typical type I curves at low relative pressure (P/P_0) and a H3 hysteresis loop according to the IUPAC classification,[19] Ru/HSAG@mSiO$_2$ also showed typical IV curves with a capillary condensation step at P/P_0 from 0.2 to 0.4. The detailed structural parameters of catalysts are listed in Table 1. The *t*-plot method at relative pressure P/P_0 from 0.3 to 0.5 was used to analyze the micro-mesopores. As a material of plate-like particle, the specific surface area of HSAG (268 m^2 g^{-1}) was comprised mainly of its plate surface area (204 m^2 g^{-1}), and the surface area of micro-mesopores (64 m^2 g^{-1}). The total pore volume (V_t) of Ru/HSAG was calculated to be 0.76 cm^3 g^{-1}, to which the contribution of

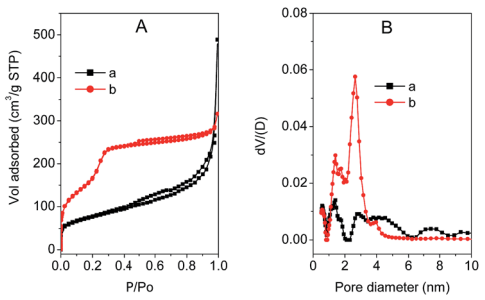

Fig. 1 Nitrogen sorption isotherms (A) and pore size distribution (B) of Ru/HSAG (a) and Ru/HSAG@mSiO$_2$ (b).

Table 1 Textural properties of Ru/HSAG and Ru/HSAG@mSiO$_2$[a]

Catalyst	S_{BET} ($m^2\ g^{-1}$)	S_m ($m^2\ g^{-1}$)	S_p ($m^2\ g^{-1}$)	V_t ($cm^3\ g^{-1}$)	V_m ($cm^3\ g^{-1}$)	Poresize (nm)	D_{Ru} (nm)	Ru content (wt%)	CO monolayer uptake (μmol g_{cat}^{-1})	D (%)
Ru/HSAG	268	64	204	0.76	0.03	—	2.6	4.0	170	43
Ru/HSAG@mSiO$_2$	613	523	90	0.49	0.33	2.7(1.3)	2.6	1.7	7.5	4.4
Ru/HSAG@mSiO$_2$-w	—	—	—	—	—	—	—	1.5	2.5	—

[a] S_{BET}: specific BET surface area; S_m: micro-mesopore surface area; S_p: $S_{BET} - S_m$; V_t: total volume; V_m: micro-mesopore volume; D_{Ru}: Ru nanoparticle size calculated by TEM; Ru content is nominal loading content; D: Ru dispersion.

micro-mesopores volume was negligible. After coated with a mesoporous silica layer, Ru/HSAG@mSiO$_2$ presented a specific surface area of 613 $m^2\ g^{-1}$, mainly resulted from micro-mesopores (523 $m^2\ g^{-1}$). This result is also confirmed by the images of SEM (Fig. 2). The surface of Ru/HSAG was rugged (Fig. 2A) but became smooth after covered with a layer of mesoporous silica as in Ru/HSAG@mSiO$_2$ (Fig. 2B).

Fig. 3 shows the TEM images of Ru/HSAG and Ru/HSAG@mSiO$_2$.Ru/HSAG exhibited a sharp-edged structure of HSAG (Fig. 3A and B), while the extremities of Ru/HSAG@mSiO$_2$ were blunt as the result of being covered with a 30 nm thickness of mesoporous silica layer (Fig. 3C and D). Ru nanoparticles with average size of 2.6 nm were selectively located at the edges of the graphite basal planes, either decorating the outer edge of graphite sheets or the steps of graphite adlayers (Fig. 3A and B). In addition, Ru nanoparticles were also well dispersed on Ru/HSAG@mSiO$_2$ without any aggregation (Fig. 3C and D). The chemical composition and structure of Ru/HSAG@mSiO$_2$ were further investigated by energy-dispersive X-ray spectroscopy (EDX) (the inset of Fig. 3C). Comparing the EDX spectra of point A1 and A2, it is clearly that the point A1 had higher concentration of silicon while lower concentration of carbon than A2, indicating the point A1 was located on the silica layer while A2 was on the overlapped area where graphite was covered by silica. The structure of Ru/HSAG@mSiO$_2$ that Ru/HSAG was encapsulated in a layer of mSiO$_2$ can thus be confirmed.

Ru nanoparticles in Ru/HSAG@mSiO$_2$ could be either embedded in the silica wall at the bottom of the pores, which made the Ru nanoparticles inaccessible to reactant molecules and led to a dramatically decline in CO monolayer uptake from 170 μmol g_{cat}^{-1} to 7.5 μmol g_{cat}^{-1} measured by CO chemisorption method (Table 1), or accessible to reactant molecules by molecule diffusion through the pores in silica layer. The later hypothesis is validated by comparison of the CO monolayer uptake of Ru/HSAG@mSiO$_2$ with Ru/HSAG@mSiO$_2$-w that had its pores blocked by residual CTAB (Table 1). Ru/HSAG@mSiO$_2$ had the CO monolayer uptake of 7.5 μmol g_{cat}^{-1} whereas Ru/HSAG@mSiO$_2$-w showed only 2.5 μmol g_{cat}^{-1}, when 10 wt% CTAB residues were in the pores of Ru/HSAG@mSiO$_2$-w.

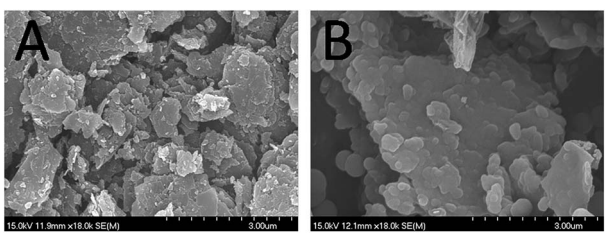

Fig. 2 SEM images of Ru/HSAG (a) and Ru/HSAG@mSiO$_2$ (b).

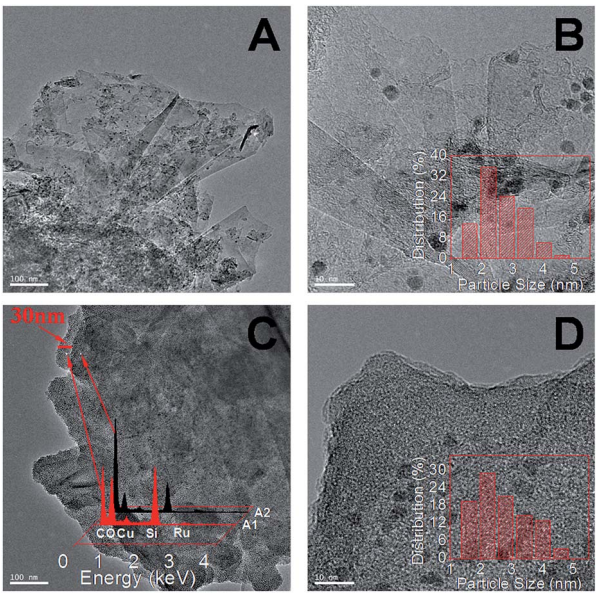

Fig. 3 TEM images of catalysts: (A and B) Ru/HSAG; (C and D) Ru/HSAG@mSiO$_2$. The insets in B and D are the Ru particle size distribution; the inset in C is the EDX of the points on two sides of the boundary of Ru/HSAG@mSiO$_2$.

Cinnamaldehyde hydrogenation

Fig. 4 shows the course of reaction during the catalytic hydrogenation of CALD (cinnamaldehyde) over catalysts. The reaction rate declined from 0.92 mol $g_{Ru}^{-1}\ h^{-1}$ on Ru/HSAG to 0.31 mol $g_{Ru}^{-1}\ h^{-1}$ on Ru/HSAG@mSiO$_2$ (Table 2), which can be attributed to the fact that part of Ru nanoparticles were capsulated in the silica wall[20] and were inaccessible to reactant molecules. The selectivity of unsaturated alcohol remained at 65% when the conversion approached to 100% on Ru/HSAG@mSiO$_2$ (see Fig. 5), while 50% of selectivity was observed over Ru/HSAG. The variation of the contents of CALD, HALD (hydrocinnamaldehyde) and HALC (hydrocinnamyl alcohol) in the reaction demonstrated that the hydrogenation of CALD to HALC *via* HALD as intermediate is a first-order consecutive reaction. On the contrary, the first-order relation was only

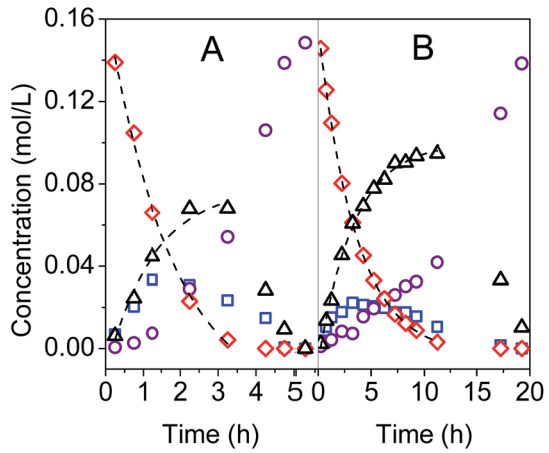

Fig. 4 Hydrogenation of CALD over the catalysts, $T = 100$ °C, $P_{H_2} = 4.0$ MPa. (A) Ru/HSAG; (B) Ru/HSAG@mSiO$_2$; (◇) CALD; (△) CALC; (□) HALD; (○) HALC. The dashes are the fitting line for CALD and CALC.

Table 2 Catalytic properties of Ru/HSAG and Ru/HSAG@mSiO$_2$ and the parameters of kinetic eqn (1)[a]

Catalyst	R (mol g_{Ru}^{-1} h^{-1})	TOF (h^{-1})	S_{60} (%)	A_0 (mol L^{-1})	k_2/k_3
Ru/HSAG	0.92	215	51	0.153	1.05
Ru/HSAG@mSiO$_2$	0.31	716	66	0.153	1.88

[a] R: average reaction rate before the conversion of CALD achieves 100%; S_{60}: selectivity of CALC when the conversion achieves 60%; TOF = RM_{Ru}/D, $M_{Ru} = 101.07$, D is Ru dispersion; A_0: the initial concentration of CALD; $T = 100$ °C, $P_{H_2} = 4.0$ MPa.

observed in the hydrogenation of CALD to CALC (cinnamyl alcohol) until the conversion of CALD achieved 100%, after which CALC started to be further hydrogenated to HALC. These reaction tends are in agreement with previous studies,[12,21] and probably imply that the cinnamaldehyde molecule containing conjugated C=C and C=O groups had the strongest adsorption on Ru sites, followed by the hydrocinnamaldehyde molecule containing an isolated C=O group and then the cinnamyl alcohol molecule containing an isolated C=C group.[22,23]

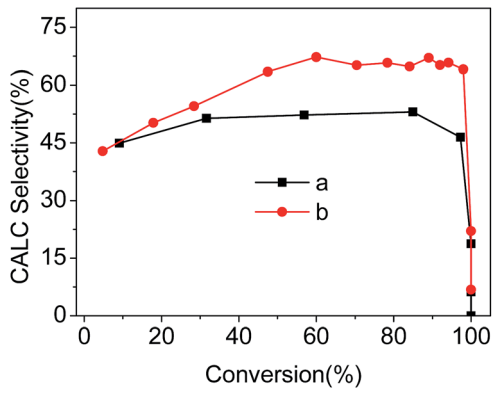

Fig. 5 The CALC selectivity of catalysts: (a) Ru/HSAG; (b) Ru/HSAG@mSiO$_2$.

Kinetic modeling

Scheme 1 shows the possible pathways of cinnamaldehyde hydrogenation. To investigate the detailed kinetics and improve the understanding of the reaction selectivity, a simplified model is presented in Scheme 2. Taking into account of the results reported in previous section, a kinetic model suitable to describe the CALD hydrogenation over catalysts has been formulated and tested. The kinetic model was developed by using rate expressions of the Langmuir–Hinshelwood type under the following assumption:[6,22]

(i) The competitive adsorption and hydrogenation of the C=C double bond and the C=O group occur on the same type of Ru sites.

(ii) The adsorption of the substrate and reaction products on the active sites is reversible and competitive.

(iii) H_2 is activated on different types of sites, and it does not compete with organic species for adsorption. The concentration of H$^\bullet$ is thus a constant.

(iv) The rate-determining step is the surface reaction between the adsorbed organic species and chemisorbed hydrogen.

Process (1) is a first-order parallel reaction with a reversible first-step, expressed by the equilibrium approximation:[24]

$$k_1 A = k_{-1} A^*$$

And the rate equation is:

$$\frac{dA}{dt} = \frac{dA^*}{dt} = k_1 A - k_{-1} A^* - k_2 A^* [H^\bullet]^2 - k_3 A^* [H^\bullet]^2$$
$$= -(k_2 + k_3)\frac{k_1}{k_{-1}} A [H^\bullet]^2$$

In process (2), the existence of A restrained the adsorption of B before the conversion of A achieved 100% (see in Fig. 4). And

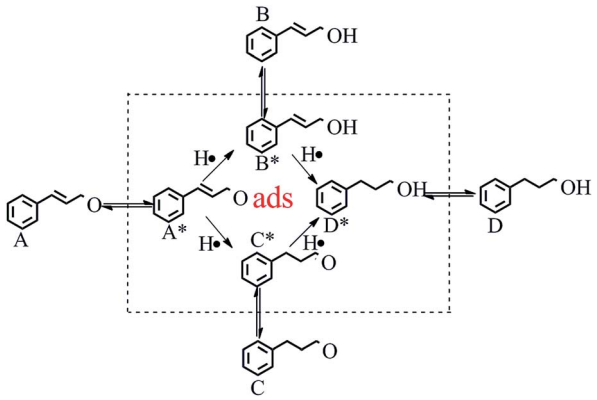

Scheme 1 The pathway of annimaldehyde hydrogenation: (A) (CALD); (B) (CALC); (C) (HALD); (D) (HALC); inside the dashed frame is the adsorption type of substrate and reaction products.

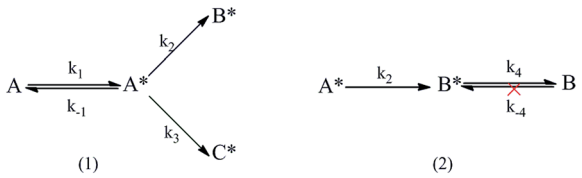

A: CALD; B: CALC; C: HALD; D: HALC

Scheme 2 The kinetic model of cinnamaldehyde hydrogenation before the cinnamaldehyde conversion achieves 100%.

the rate-determining step is: $A^* \rightarrow B^*$, using the steady state approximation,[24] the rate equation for B^* is:

$$\frac{dB^*}{dt} = -k_2 A^*[H^\cdot]^2 + k_4 B^* = 0$$

As a competitive reaction, the equation for the selectivity of B is:

$$S = \frac{k_2}{k_2 + k_3}$$

And the rate equation for B is:

$$\frac{dB}{dt} = k_4 B^* = k_2 A^*[H^\cdot]^2 = k_2 \frac{k_1}{k_{-1}} A[H^\cdot]^2$$

$$= k_2 \frac{k_1}{k_{-1}} \left(A_0 - \frac{B}{S}\right)[H]^2$$

$$= k_2 \frac{k_1}{k_{-1}} A_0[H^\cdot]^2 - \frac{k_1(k_2 + k_3)}{k_{-1}} B[H^\cdot]^2$$

where A_0 is the initial concentration of CALD.

When $t = 0$, $B = 0$ mol L^{-1}, it gives

$$B = -\frac{k_2}{k_2 + k_3} A_0 e^{-\frac{k_1(k_2+k_3)}{k_{-1}}[H^\cdot]^2 t} + \frac{k_2}{k_2 + k_3} A_0 \quad (1)$$

When the eqn (1) was used to fit the concentration curve of CALC in Fig. 4, the Adj. R-square (coefficient of determination) was determined to be 0.96 and 0.99 for Ru/HSAG and Ru/HSAG@mSiO_2, respectively. It indicates that this kinetic model and the assumptions are suitable to describe the process of cinnamaldehyde hydrogenation on these catalysts. This kinetic model also supported the fact that there was a competitive adsorption between CALD and CALC on Ru surface and the existence of CALD restrained the adsorption of CALC before the conversion of CALD achieved 100%. Since the cinnamaldehyde hydrogenation is a parallel reaction, the ratio of reaction rate constant (k_2/k_3) indicates the selectivity of CALC. The calculated values of k_2/k_3 are 1.05 and 1.88 on Ru/HSAG and Ru/HSAG@mSiO_2, respectively (see Table 2), which are consistent with the values obtained experimentally from Fig. 5.

Discussion

The electronic property of supports and the geometric structure of metals are two key factors of catalysts influencing the selectivity of cinnamaldehyde hydrogenation. Compared to other supports, the selectivity was much higher on graphite because of a charge transfer from the support to the metal, which increased the charge density on metal, thus decreasing the probability for the C=C bond activation.[18] When the type of supports was chosen, as the case of our study using high surface area graphite as support, the geometric structure of catalyst played an important role in determining the selectivity in reactions. One of the geometric effects that metals have is the particle size, as we know there is a steric hindrance for the C=C bond adsorption on a flat surface,[8,11,12,25] which however can be ruled out in our case as the particle size of Ru nanoparticles maintained at 2.6 nm (see TEM images in Fig. 3) before and after being covered with the mSiO_2 layer. Another geometric effect imposed on the selectivity of cinnamaldehyde hydrogenation originates from the confinement of metals in pores. We have demonstrated that Ru/HSAG@mSiO_2, in which Ru nanoparticles were supported on graphite and confined at the bottom of silica pores, was able to deliver 15% higher selectivity than its unconfined counterpart. The schematic illustration of the influence of confinement of metals by mSiO_2 layers on the selective hydrogenation of cinnamaldehyde is presented in Fig. 6. As a shape-selective layer, the pores in silica layer determined the adsorption mode of cinnamaldehyde molecules on Ru nanoparticles. To reach the Ru surface, CALD molecules should first diffuse through the pores of mSiO_2 layer. With a branching chain in CALD molecule, the length of CALD is longer than its width. In pores with average pore size of 2.7 nm, the possibility of flat-on adsorption of CALD molecules on Ru surface was reduced, as a result of which less C=C bonds were hydrogenated, the hydrogenation of terminal C=O bond was thus favored. In this way, the selectivity of CALC (unsaturated alcohol) in cinnamaldehyde hydrogenation was improved. On the other hand, the TOF value on Ru/HSAG@mSiO_2 was also significantly enhanced (three times higher than that on Ru/HSAG), which was due to the fact that the flat-on CALD molecules cover more active sites on Ru nanoparticles than the molecules with end-on adsorption (Table 2). To the best of our knowledge, this is the first report investigating the geometric effect of catalysts after ruling out the influences from other factors, namely, electronic property of supports and particle size of metals.

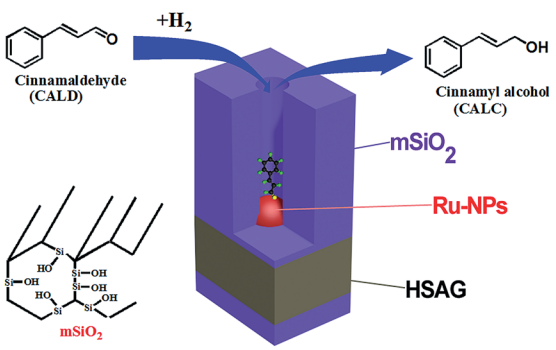

Fig. 6 The geometric effect of Ru/HSAG@mSiO_2 for CALD hydrogenation to unsaturated alcohol.

Conclusions

A general strategy for the facile preparation of graphite-supported metal nanoparticles encapsulated by mesoporousm SiO_2 layers has been developed. Ru nanoparticles were supported on high surface area graphite and were confined at the bottom of silica pores. The special geometric structure enhanced the hydrogenation of the C=O bond of cinnamaldehyde to unsaturated alcohol as well as turnover frequency (TOF). The pore size of $mSiO_2$ layers can be tailored through changing the length of alkyl chain of the cationic surfactants[26] or silylation with organosilanes with variable chain lengths,[27] to further improve the selectivity of CALC. The synthetic strategy can also be extended to other graphite-supported catalysts containing metals, such as Pt and Pd, for various selective catalytic reactions.

Acknowledgements

The financial support from the National Natural Science Foundation of China (NSFC Grant no. 21303163), the Qianjiang Talent Project in Zhejiang Province (QJD1302011) and the Scientific Research Fund of Zhejiang Provincial Education Department (Y201328681) are gratefully acknowledged.

Notes and references

1 Y. Wan and D. Zhao, *Chem. Rev.*, 2007, **107**, 2821–2860.
2 N. Tiengchad, O. Mekasuwandumrong, C. Na-Chiangmai, P. Weerachawanasak and J. Panpranot, *Catal. Commun.*, 2011, **12**, 910–916.
3 C. Li, H. Zhang, D. Jiang and Q. Yang, *Chem. Commun.*, 2007, 547.
4 X. Pan and X. Bao, *Acc. Chem. Res.*, 2011, **44**, 553–562.
5 T. Maschmeyer, F. Rey, G. Sankar and J. M. Thomas, *Nature*, 1995, **378**, 159–162.
6 P. Mäki-Arvela, J. Hájek, T. Salmi and D. Y. Murzin, *Appl. Catal., A*, 2005, **292**, 1–49.
7 P. Gallezot, A. Giroir-Fendler and D. Richard, *Catal. Lett.*, 1990, **5**, 169–174.
8 A. Giroir-Fendler, D. Richard and P. Gallezot, *Catal. Lett.*, 1990, **5**, 175–181.
9 W. Yu, H. Liu, M. Liu and Q. Tao, *J. Mol. Catal. A: Chem.*, 1999, **138**, 273–286.
10 A. Chambers, S. David Jackson, D. Stirling and G. Webb, *J. Catal.*, 1997, **168**, 301–314.
11 S. Galvagno, G. Capannelli, G. Neri, A. Donato and R. Pietropaolo, *J. Mol. Catal.*, 1991, **64**, 237–246.
12 S. Galvagno, C. Milone, G. Neri, A. Donato and R. Pietropaolo, in *Studies in Surface Science and Catalysis*, 1993, vol. 78, pp. 163–170.
13 L.-P. Tiainen, P. Mäki-Arvela, A. K. Neyestanaki, T. Salmi and D. Y. Murzin, *React. Kinet. Catal. Lett.*, 2003, **78**, 251–257.
14 P. N. Rylander, *Catalytic hydrogenation in organic syntheses*, Academic Press, New York, 1979.
15 M. Lashdaf, A. O. I. Krause, M. Lindblad, M. Tiitta and T. Venäläinen, *Appl. Catal., A*, 2003, **241**, 65–75.
16 J. Hájek, N. Kumar, P. Mäki-Arvela, T. Salmi, D. Y. Murzin, I. Paseka, T. Heikkilä, E. Laine, P. Laukkanen and J. Väyrynen, *Appl. Catal., A*, 2003, **251**, 385–396.
17 J. Planeix, N. Coustel, B. Coq, V. Brotons, P. Kumbhar, R. Dutartre, P. Geneste, P. Bernier and P. Ajayan, *J. Am. Chem. Soc.*, 1994, **116**, 7935–7936.
18 A. Giroir-Fendler, D. Richard and P. Gallezot, *Stud. Surf. Sci. Catal.*, 1988, **41**, 171–178.
19 S. J. Gregg, K. S. W. Sing and H. W. Salzberg, *J. Electrochem. Soc.*, 1967, **114**, 279C.
20 L. Shang, T. Bian, B. Zhang, D. Zhang, L. Z. Wu, C. H. Tung, Y. Yin and T. Zhang, *Angew. Chem., Int. Ed.*, 2014, **53**, 250–254.
21 Z. Sun, Z. Rong, Y. Wang, Y. Xia, W. Du and Y. Wang, *RSC Adv.*, 2014, **4**, 1874–1878.
22 G. Neri, L. Bonaccorsi, L. Mercadante and S. Galvagno, *Ind. Eng. Chem. Res.*, 1997, **36**, 3554–3562.
23 S. Galvagno, C. Milone, A. Donate, G. Neri and R. Pietropaolo, *Catal. Lett.*, 1993, **18**, 349–355.
24 L. Volk, W. Richardson, K. H. Lau, M. Hall and S. H. Lin, *J. Chem. Educ.*, 1977, **54**, 95.
25 P. Gallezot and D. Richard, *Catal. Rev.*, 1998, **40**, 81–126.
26 C. T. Kresge, M. E. Leonowicz, W. J. Roth, J. C. Vartuli and J. S. Beck, *Nature*, 1992, **359**, 710–712.
27 H. Yang, Y. Chong, X. Li, H. Ge, W. Fan and J. Wang, *J. Mater. Chem.*, 2012, **22**, 9069.